

# Effects of melamine phosphate on the thermal decomposition and combustion behavior of reconstituted tobacco sheet

Shun Zhou · Min Ning · Yingbo Xu · Junsheng Shu ·  
Chenghui Wang · Yuan Hu · Shaolin Ge · Zhenfeng Tian ·  
Shike She · Qing He

Received: 14 May 2012 / Accepted: 30 August 2012 / Published online: 2 October 2012  
© Akadémiai Kiadó, Budapest, Hungary 2012

**Abstract** In this paper, first the MP-modified reconstituted tobacco sheet (RTS) was prepared by a paper-making process. Thermogravimetric analysis coupled to Fourier transform infrared spectrometer (TG-FTIR) had been used to investigate the influences of melamine phosphate (MP) on the thermal decomposition and the formation of evolved volatile products of RTS. TG-FTIR results illustrated that the incorporation of MP into RTS could retard the thermal decomposition of the major components of RTS and meanwhile lead to the formation of more thermally stable char. Moreover, the main gases released during the pyrolysis of RTS and MP-modified RTS were H<sub>2</sub>O, CO<sub>2</sub>, CO, NH<sub>3</sub>, carbonyl compounds, alcohols, phenols, alkanes, and alkenes. The presence of MP changed the formation of evolved volatile products of RTS obviously. The effects of MP on the combustion behavior of RTS were studied by micro-scale combustion calorimetry and cone calorimetry. Results demonstrated that the formation of combustible

gases was mainly determined by the thermal decomposition stage occurred in the temperature range of 150–600 °C. The incorporation of MP into RTS influenced the release of fuel gases and the char formation in the process of the thermal decomposition of RTS, and eventually retarded the flammability and combustibility of RTS.

**Keywords** Reconstituted tobacco sheet · Combustion · TG-FTIR · Micro-scale combustion calorimetry · Cone calorimetry

## Introduction

Reconstituted tobacco sheet (RTS), due to its advantageous economic impact on the manufacturing cost of cigars and cigarettes, has been widely used by the tobacco industry [1]. RTS can be usually produced by tobacco that cannot be incorporated directly into cigarettes, such as tobacco dust, mid-ribs and leaf scraps [2]. Compared with the starting tobacco, the reconstitution processes always lead to some loss of natural constituents of the tobacco, yielding an adverse smoke flavor. As a result, some additives are necessary to be incorporated into the reconstituted tobacco sheet during the manufacturing process for flavoring, process conditioning, and reduction of harshness and irritation [3].

Diammonium phosphate (DAP) has been historically used as ingredients added to reconstituted tobacco sheet, to increase free nicotine “delivery” in cigarettes, highlight certain flavors and release the pectins in tobacco stems so they may form a gel which becomes the binder in the blended leaf sheet [4]. It is noteworthy that DAP also can be used as flame retardants, especially in the intumescent flame retarded system (IFRS). A typical IFRS comprises an

---

S. Zhou (✉) · M. Ning (✉) · Y. Xu · J. Shu · C. Wang ·  
S. Ge · Z. Tian · S. She · Q. He  
Research and Development Centre, China Tobacco Anhui  
Industrial Co., Ltd., 9 Tianda Road, Hefei 230088,  
Anhui, People’s Republic of China  
e-mail: zhous@mail.ustc.edu.cn

M. Ning  
e-mail: tobacco\_shun@163.com

S. Zhou · M. Ning · Y. Xu · S. Ge · Z. Tian  
CTAH-USTC Joint Research Laboratory for Tobacco  
Chemistry, 9 Tianda Road, Hefei 230088, Anhui,  
People’s Republic of China

Y. Hu  
State Key Laboratory of Fire Science, University of Science  
and Technology of China, 96 Jinzai Road, Hefei 230026,  
Anhui, People’s Republic of China

acid source—a dehydration catalyst for char formation, a carbon source—a carbonization agent and a gas source—a blowing agent [5]. DAP can release phosphoric acid and incombustible gases during its thermal degradation process, and thus has been usually used as acid source and gas source in the IFRS. As a matter of fact, DAP has been extensively used to improve the flame retardation of biomass [6], bio-composites [7], and fabrics [8]. Similarly, melamine phosphate (MP), as a typical intumescent flame retardant, also has been widely used to enhance the flame retardation of polymers, such as polypropylene, polyamides, and epoxy resins, etc [9–11]. However, little publications have been found on the use of MP in RTS manufacturing processes compared to DAP. RTS, as an integral part of the cigarette, is combusted and pyrolyzed in a burning cigarette. Doubtless, the incorporation of MP would influence the pyrolysis and combustion properties of RTS definitely. Nevertheless, little studies pertaining to the influences of MP on the pyrolysis and combustion behavior of RTS could be found.

In the present study, RTS and the MP-modified RTS are prepared by a paper-making process. Thermogravimetric analysis coupled to Fourier transform infrared spectrometer (TG-FTIR) has been used to investigate the influences of MP on the thermal decomposition and the formation of evolved volatile products of RTS. Moreover, the effects of MP on the combustion behavior of RTS are studied by micro-scale combustion calorimetry (MCC) and cone calorimetry (CCO).

## Experimental

### Materials

MP was supplied by Hefei Jinhui Institute of Chemical Engineering, China. The  $d_{50}$ -value for the particle size distribution of MP was  $61.3 \mu$ . Pure RTS and MP-modified RTS were manufactured by a papermaking process. Detailedly speaking, in the papermaking process, the water-soluble fraction of the tobacco scrap was first extracted, leaving behind a tobacco pulp. The resulting pulp was mechanically beaten to fibrillate the cellulose and reduce its fiber length. The refined cellulose was then formed into a web on the wire screen of a standard papermaking machine and dried by suction and hot air. In a parallel operation, the tobacco extract was concentrated. The cellulose web was impregnated with the concentrated tobacco extract (as for MP-modified RTS, 5 kg MP was added into 40 L of the concentrated tobacco extract) and then dried, consequently RTS and MP-modified RTS could be obtained.

### Measurements

#### *Scanning electron microscopy (SEM) and energy dispersive X-ray spectroscopy (EDX)*

The morphology and elemental composition of RTS and MP-modified RTS were investigated using field-emission scanning electron microscopy (FE-SEM, Siron 200, Netherlands) with EDX (Oxford, UK).

#### *TG-FTIR*

Thermogravimetric/infrared spectrometry analysis was performed using TGA Q5000 IR thermogravimetric analyzer that was interfaced to the Nicolet 6700 FTIR spectrophotometer. About 30 mg of RTS sample was put in an alumina crucible and heated from 30 to 950 °C at a heating rate of 30 °C min<sup>-1</sup> under the flow of 10 % oxygen in nitrogen. The pyrolysis products generated from the TG furnace were introduced into the gas cell of the FTIR analyzer by nitrogen with a flow rate at 60 mL min<sup>-1</sup>. The line that transferred the evolved gases from the TG to the FTIR and the IR cell was maintained at 225 and 230 °C, respectively. The FTIR was operated in the continuous scan mode covering 4,000–500 cm<sup>-1</sup> at a resolution of 4 cm<sup>-1</sup>.

#### *Micro-scale combustion calorimetry*

The MCC measurement was performed by an “MCC-2” micro-scale combustion calorimeter produced by Govmark, Farmingdale, New York. The RTS sample, approximately 4 mg, was heated to a specified temperature (i.e., 650 °C) using a heating rate of 30 °C min<sup>-1</sup>, in a stream of nitrogen flow at 90 cm<sup>3</sup> min<sup>-1</sup>. The thermal degradation products were mixed with a 10 cm<sup>3</sup> min<sup>-1</sup> stream of oxygen prior to entering a 900 °C combustion furnace.

#### *Cone calorimetry (CCO)*

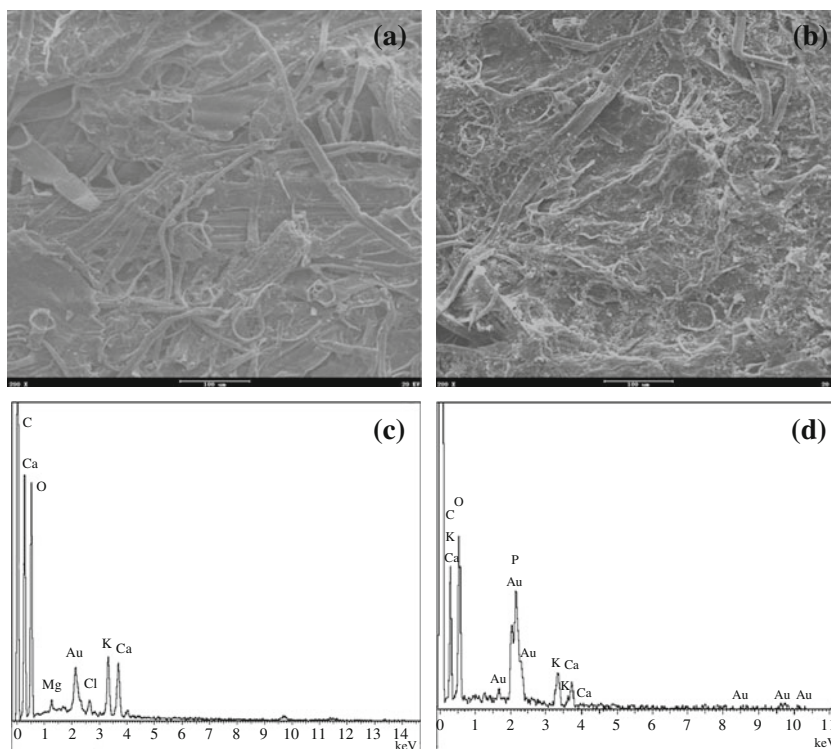
The cone calorimeter (Stanton Redcroft, UK) tests were performed on the basis of ISO 5660 standard procedures. Each specimen of dimensions 100 × 100 × 0.2 mm<sup>3</sup> was wrapped in aluminum foil and exposed horizontally at an external heat flux of 35 kW m<sup>-2</sup>.

## Results and discussions

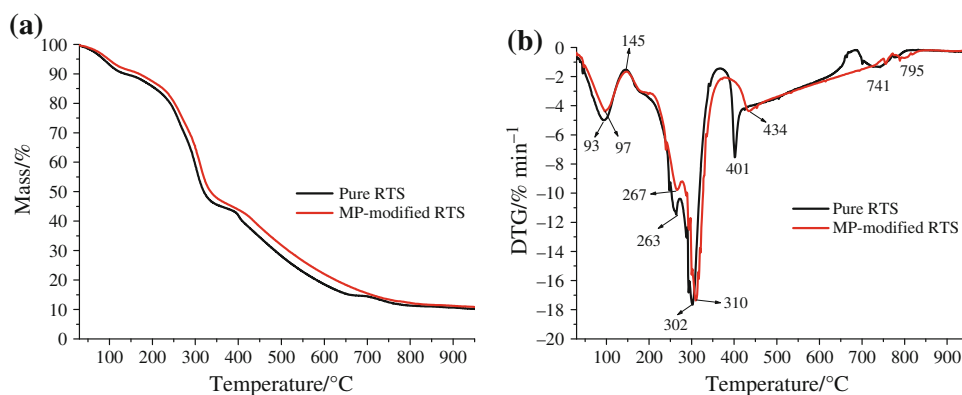
### Morphology of RTS and APP-modified RTS

Figure 1 shows the SEM images and EDX spectra of RTS and MP-modified RTS. From SEM images (Fig. 1a, b), it

**Fig. 1** SEM images and EDX spectra of the surface for **a**, **c** RTS and **b**, **d** MP-modified RTS



**Fig. 2** **a** TG and **b** DTG curves of pure RTS and MP-modified RTS



can be seen that the surface of MP-modified RTS contains more particles in comparison with that of pure RTS. Moreover, the results of the EDX elemental microanalyses show that the elements on the surface of pure RTS are mainly C, O, Ca, K, Cl, Mg, etc. For MP-modified RTS, one intensive peak appears corresponding to P elements, indicating the existence of MP.

The thermal decomposition of pure RTS and MP-modified RTS

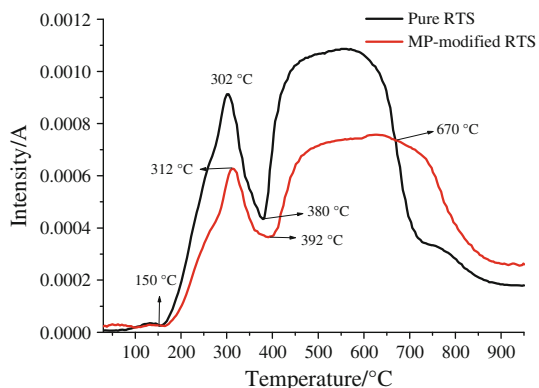
Figure 2a and b present TG and DTG curves obtained from the thermal decomposition of pure RTS and MP-modified RTS under the atmosphere of 10 % O<sub>2</sub> in nitrogen, respectively. The onset degradation temperature of samples was evaluated by the temperature of 5 wt% mass loss

( $T_{-5\%}$ ); the mid-point temperature of the degradation ( $T_{-50\%}$ ), and the solid residue left at 900 °C were obtained from the TG curve; the temperature of the maximum mass loss rate ( $T_{\max}$ ) of samples was obtained from the DTG curve. These data are listed in Table 1.

As for neat RTS, its TG and DTG curves mainly show five mass loss stages. The first stage with a light mass loss of 11.0 % takes place in the temperature range of 40–150 °C, mainly corresponding to the loss of water and volatile species. It is followed by the two sharp mass losing stages occurred at 200–280 and 280–370 °C, respectively, leading to 44.1 % mass loss totally. This is due to the thermal degradation of some major constituent of reconstituted tobacco sheet (i.e., cellulose, hemicellulose, lignin, pectin, etc.) with the evolution of various gaseous products and the formation of solid char [12–15]. The following

**Table 1** TG data of pure RTS and MP-modified RTS

Sample	$T_{-5} \text{ } ^\circ\text{C}$	$T_{-50} \text{ } ^\circ\text{C}$	$T_{\text{max}} \text{ } ^\circ\text{C}$	Residual mass (at 900 °C) /%
Pure RTS	86	320	302	10.58
MP-modified RTS	94	336	310	11.24

**Fig. 3** The Gram–Schmidt curves of the total FTIR absorbance intensity of evolved gases gotten during the pyrolysis of per milligram pure RTS and MP-modified RTS in TG-FTIR tests

thermal degradation process from 370 to 670 °C is caused by the thermal decomposition of char [16]. After 680 °C, the thermal decomposition of  $\text{CaCO}_3$  and other salts results in the appearance of the last mass losing stage. The residual mass at 900 °C is 10.58 %.

Compared the TG curve of MP-modified RTS with that of RTS, it is clearly seen that the presence of MP changes the thermal degradation behavior of RTS obviously. According to Fig. 2a and Table 1, the data of  $T_{-5} \%$ ,  $T_{-50} \%$  and the residual mass at 900 °C of MP-modified RTS are higher than those of RTS, indicating that the incorporation of MP into RTS could improve the thermal stability of RTS. As shown in Fig. 2b, the DTG curve of MP-modified RTS is different from that of RTS, though it mainly consists of five mass loss stages as well. To be specific, in terms of the second mass losing stage in the temperature range of 200–280 °C, for MP-modified RTS, the peak of mass loss rate is  $9.77 \text{ } \% \text{ min}^{-1}$  at 267 °C instead of  $11.4 \text{ } \%/ \text{min}$  at 263 °C for virgin RTS. During the mass loss stage occurred between 280–370 °C, the  $T_{\text{max}}$  value of RTS is 302 °C, while that for MP-modified RTS is 312 °C. Moreover, compared to neat RTS, the temperature corresponding to the maximal mass loss rate appeared in the fourth mass loss step of MP-modified RTS is enhanced from 401 to 434 °C. According to the above analysis, it is noted that the incorporation of MP into RTS could retard the thermal decomposition of the major components of

RTS and meanwhile lead to the formation of more thermally stable char.

#### FTIR analysis of pyrolysis gases

Figure 3 shows the Gram–Schmidt curves of the total FTIR absorbance intensity of gaseous products gotten during the pyrolysis of per milligram pure RTS and MP-modified RTS by TG-FTIR. It can be seen from Fig. 3 that the Gram–Schmidt curves of pure RTS and MP-modified RTS mainly consist of three steps. Comparison of Gram–Schmidt curve with DTG curve indicates that the temperature of the IR absorbance peaks is in agreement with that of the DTG peaks, although the DTG curve has two more peaks than the Gram–Schmidt curve. Before 150 °C, the first step of Gram–Schmidt plot is corresponding to the initial thermal decomposition stage of DTG curve. The second and third mass loss stages in DTG curve play the most important role in determining the formation of the second step of Gram–Schmidt plot. The appearance of the third step of Gram–Schmidt plot is due to the last two thermal decomposition stages of DTG curves. Compared to neat RTS, the intensity of the Gram–Schmidt curve for MP-modified RTS is relatively weaker when the temperature is below 670 °C, illustrating that the amount of evolved gas for MP-modified RTS in this stage is lower than that for neat RTS.

The 3D FTIR spectra (absorbance–wavenumber–minutes) of the gaseous products obtained from the pyrolysis of pure RTS and MP-modified RTS is showed in Fig. 4. As shown in Fig. 4, it is clear that there are mainly following absorption regions, i.e., 3786–3443, 3130–2670, 2400–2226, 2220–2000, 1850–1580, 1570–1250, 1500–1300, 1240–830, and 770–590  $\text{cm}^{-1}$ , which could be observed from the 3D FTIR spectra. Although it is difficult to identify every species in the mixture of gas products for the overlapping of their IR absorbance, some gas products with very specific IR absorption can be identified easily. The detection of carbon dioxide in the absorption region of 2,400–2,226  $\text{cm}^{-1}$  is undoubted, and it is also confirmed by the absorption peak at 672  $\text{cm}^{-1}$  [17]. The attribution of the peaks at 2,180 and 2,110  $\text{cm}^{-1}$  to carbon monoxide is also definite [17]. The absorption peaks at 3,730 and 1,508  $\text{cm}^{-1}$  are well known to be due to the absorptions of water vapor [18]. Moreover, the adsorption band at 965  $\text{cm}^{-1}$  has been widely used to determine the existence of  $\text{NH}_3$  [19]. The presence of alkene compounds are indicated by the IR bands at 3,090  $\text{cm}^{-1}$ , typical stretching vibrations of  $=\text{C}-\text{H}$  and the absorption bands at 1,650  $\text{cm}^{-1}$ , due to the  $\text{C}=\text{C}$  stretching vibrations, illustrating the existence of ethene. The bands between 3,000–2,770 and 1,500–1,300  $\text{cm}^{-1}$  are an indication of the presence of aliphatic species such as  $-\text{CH}_3$  and  $-\text{CH}_2-$ , of which methane is the most abundant [20]. The bands between 1,850 and 1,660  $\text{cm}^{-1}$ , ascribed to the  $\text{C}=\text{O}$  group

**Fig. 4** The 3D surface graph for the FTIR spectra of the evolved gases produced by the pyrolysis of **a** pure RTS and **b** MP-modified RTS in TG-FTIR tests

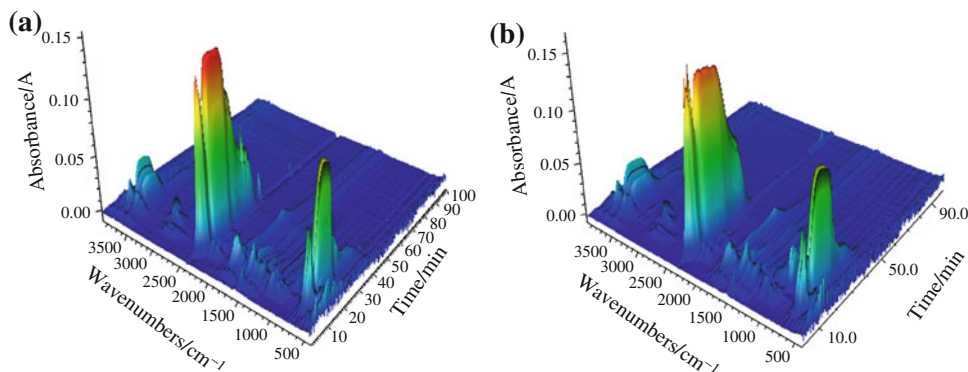
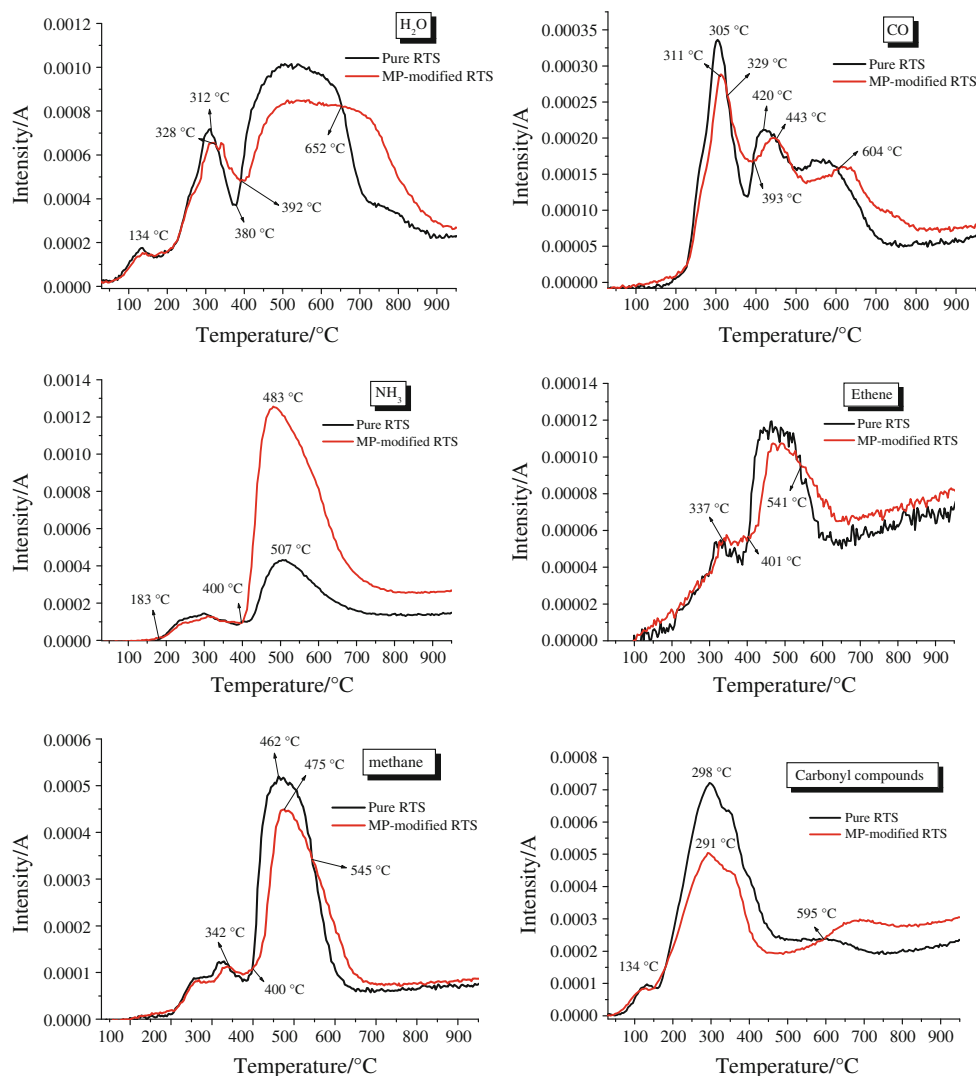


**Fig. 5** Evolution of H<sub>2</sub>O, CO, NH<sub>3</sub>, ethene, methane, and carbonyl compounds evolved from the pyrolysis of per milligram pure RTS and MP-modified RTS measured by TG-FTIR experiments



of carbonyl compounds, indicate the release of some organics, including aldehydes, acids, ketones, anhydrides, etc [21]. The intense bands at 1,100–930 cm<sup>-1</sup> are attributable to the stretching of C–O bonds from alcohols. In particular, the peak at 1,056 cm<sup>-1</sup>, assigned to the typical absorption of primary alcohols, denotes the presence of methanol [22]. Consequently, according to the above

analysis, it is noted that the main gases released during the pyrolysis of RTS and MP-modified RTS are H<sub>2</sub>O, CO<sub>2</sub>, CO, NH<sub>3</sub>, carbonyl compounds (such as aldehydes, ketones, and acids), alcohols, phenols, alkanes, and alkenes.

Figure 5 shows the evolution curves of some of the main gaseous products, i.e., H<sub>2</sub>O, CO, NH<sub>3</sub>, ethene, methane, and carbonyl compounds, from the pyrolysis of per

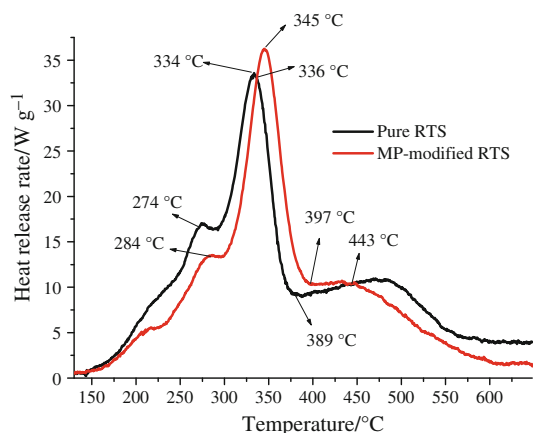


**Fig. 6** HRR versus temperature curves of pure RTS and MP-modified RTS during MCC tests

**Table 2** MCC data of pure RTS and MP-modified RTS

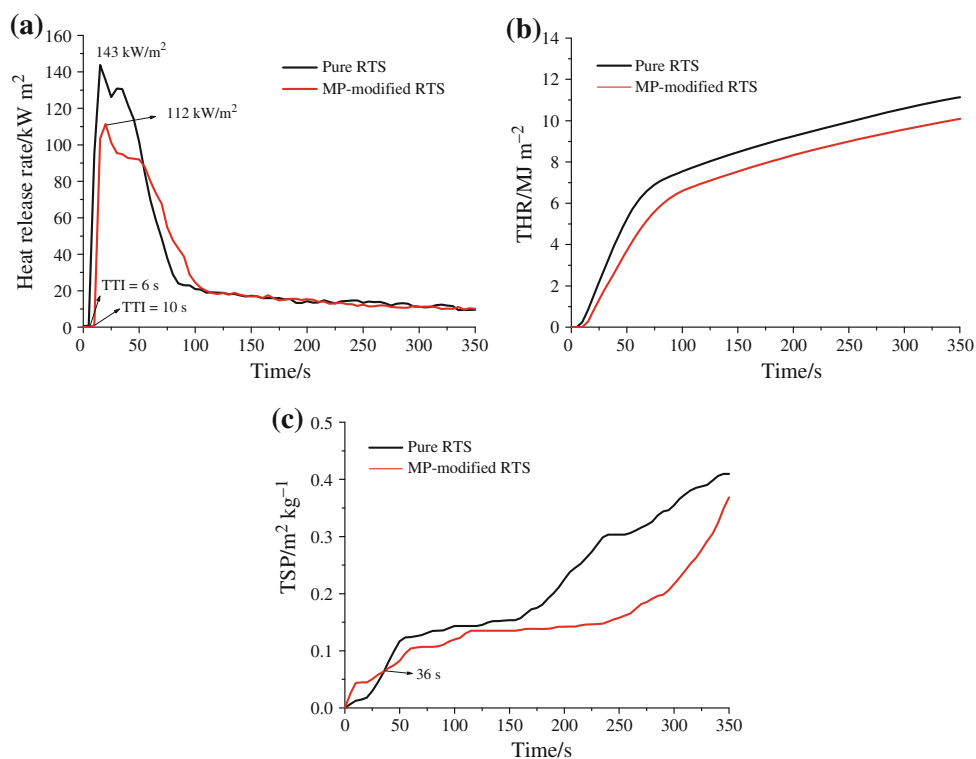
Sample	PHRR /W g <sup>-1</sup>	THR /kJ g <sup>-1</sup>	Ignition temperature /°C
Pure RTS	32.9	4.9	330.2
MP-modified RTS	36.3	3.8	343.6

milligram pure RTS and MP-modified RTS. As for virgin RTS, only little H<sub>2</sub>O and carbonyl compounds could be found in the curves when the pyrolysis temperature is

below 200 °C, since the absorbed water and volatile carbonyl compounds are released out by evaporation. When the temperature is beyond 200 °C, H<sub>2</sub>O, CO, ethene, methane, and carbonyl compounds form quickly with the extensive thermal degradation of saccharide ingredients (such as sugars, celluloses, starch, and gums), which are some major constituent of reconstituted tobacco sheet. It is noteworthy that the further thermal decomposition of the char formed in the third mass loss stage also can lead to the formation of CO and H<sub>2</sub>O at relatively higher temperature. With regard to NH<sub>3</sub>, the release of NH<sub>3</sub> is primarily due to the thermal decomposition of nitrogen-containing compounds in tobacco, such as protein, amino acid, amine salt, nicotine, nitrate, and tobacco-specific nitrosamines, etc [23].

Release of H<sub>2</sub>O, CO, NH<sub>3</sub>, ethene, methane, and carbonyl compounds during the thermal decomposition of MP-modified RTS generally follows a similar trend to that of neat RTS. However, with the exception of NH<sub>3</sub>, by comparing the intensity of the peak release rates for H<sub>2</sub>O, CO, ethene, methane, and carbonyl compounds, it can be observed that the peak of release rate for MP-modified RTS is lowered as compared to the untreated RTS. It is interesting to compare the formation of NH<sub>3</sub> for pure RTS with that for MP-modified RTS. As seen from Fig. 5, the formation process of NH<sub>3</sub> is mainly composed of two stages. The first stage appears in the temperature range of 183–400 °C. In this stage, the release intensity of NH<sub>3</sub> for MP-modified RTS is relatively weaker in comparison with

**Fig. 7** **a** HRR, **b** THR, and **c** TSP release rate curves of the modified RTS versus pure RTS under a heat flux of 35 kW m<sup>-2</sup> during CCO tests



that for pure RTS. However, when the temperature is above 400 °C, the release intensity of NH<sub>3</sub> for MP-modified RTS increases sharply and becomes far stronger than that for pure RTS. This is quite reasonable when taking into consideration that the thermal decomposition of MP itself. As a matter of fact, these transformations could be caused by a progressive condensation of the melamine groups in MP with the elimination of NH<sub>3</sub>. According to the literature, at above 250 °C, melamine is condensed to melam, melem, and melon with the increase of the temperature [24].

#### Combustion behavior of RTS and MP-modified RTS

MCC, as a pyrolysis combustion flow calorimeter using controlled pyrolysis and complete combustion of the fuel gases, can provide a convenient methodology for evaluating the combustion and pyrolysis properties of pure RTS and MP-modified RTS [25]. Fig. 6 shows heat release rate (HRR) versus temperature curves of pure RTS and MP-modified RTS. The data of peak heat release rate (PHRR), total heat release (THR), and ignition temperature are listed in Table 2. As for pure RTS, it starts to decompose and form fuel gases at 150 °C as shown by an increase in HRR curve. The HRR value reaches its maximum (32.9 W g<sup>-1</sup>) at 334 °C (i.e., ignition temperature) and then decreases quickly to 9.0 W g<sup>-1</sup> when temperature is up to 380 °C. With the further increase of temperature, a relatively small peak appears at 478 °C in the HRR curve, obviously resulting from the thermal decomposition of char. Then HRR curve ends at 600 °C, illustrating that the termination of pyrolytic formation of fuel gases. Comparison of HRR curve with DTG curve indicates that the formation of fuel gases is mainly determined by the thermal decomposition stage of RTS occurred in the temperature range of 150–600 °C.

In terms of MP-modified RTS, it is clearly seen from Fig. 6 that the trend of the HRR curve for MP-modified RTS is quite similar to that for neat RTS. However, when temperature is below 336 °C, at the same temperature, the HRR value of MP-modified RTS is lower in contrast with that of neat RTS, demonstrating that the incorporation of MP into RTS limits the release of fuel gases in this temperature range. In the temperature ranged from 336 to 443 °C, it is interesting to see that the HRR value of MP-modified RTS become bigger than that of neat RTS. This demonstrates that MP-modified RTS releases more combustible gases (such as CO, ethene, and methane, as showed in Fig. 5) in this temperature range compared to neat RTS. When temperature is above 443 °C, the HRR value of virgin RTS is higher than that of MP-modified RTS, indicating that the char formed during the thermal decomposition of MP-modified RTS is relatively more stable. Moreover, as showed in Table 2, the THR of MP-modified RTS is lower than that of neat RTS,

suggesting that the combustibility of RTS is retarded by the incorporation of MP. This also can be testified by the results obtained from cone calorimeter tests.

Cone calorimeter testing can provide a wealth of information on the combustion behavior of materials under controlled levels of radiant heating [26]. The HRR, THR, and total smoke production (TSP) curves of the modified RTS versus RTS under a heat flux of 35 kW m<sup>-2</sup> are showed in Fig. 7. HRR, in particular the peak HRR (PHRR), has been found to be one of the most important parameters to evaluate the flammability of materials. As seen from Fig. 7a, the neat RTS burns very fast after ignition, and a sharp RHR peak appears with a PHRR value of 143 kW m<sup>-2</sup>. In the case of the MP-modified RTS, its PHRR value is reduced to 112 kW m<sup>-2</sup>. Moreover, the time to ignition of MP-modified RTS is prolonged in comparison with that of virgin RTS. Figure 7b gives the THR curves of neat RTS and MP-modified RTS, it is noticeable that the THR value of neat RTS is higher than that of MP-modified RTS at the same time in the process of the whole combustion. At the end of burning, pure RTS has released a total heat of 11.1 MJ m<sup>-2</sup>, whereas MP-modified RTS only released 10.0 MJ m<sup>-2</sup>. The experimental data above confirms that the flammability of MP-modified RTS is markedly lower than that of neat RTS. Another important parameter that helps the understanding of the combustion related to materials is emission of smoke. As showed in Fig. 7c, the TSP value of pure RTS is lower than that of MP-modified RTS, because pure RTS is rapidly burned at early stage of combustion. After an ignition time of 36 s, pure RTS produces more smoke in comparison with MP-modified RTS, indicating that MP has a smoke suppression effect.

#### Conclusions

TG-FTIR results illustrated that the incorporation of MP into RTS can retard the thermal decomposition of the major components of RTS and meanwhile lead to the formation of more thermally stable char. Moreover, the main gases released during the pyrolysis of RTS and MP-modified RTS were H<sub>2</sub>O, CO<sub>2</sub>, CO, NH<sub>3</sub>, carbonyl compounds, alcohols, phenols, alkanes, and alkenes. The presence of MP changed the formation of evolved volatile products of RTS obviously. MCC and CCO results showed that the formation of combustible gases were mainly determined by the thermal decomposition stage occurred in the temperature range of 150–600 °C. The incorporation of MP into RTS influenced the release of fuel gases and the char formation in the process of the thermal decomposition of RTS, and eventually retarded the flammability and combustibility of RTS obviously.

**Acknowledgements** The financial supports from China National Tobacco Corporation (No: 110200902012 and 110200901002) and China Tobacco Anhui Industrial Corporation (No: 20111004) are acknowledged.

## References

- Browne CL. The design of cigarettes, vol. 3. Charlotte: Hoechst Celanese Corporation; 1990.
- Borgerding MF, Perfetti TA, Ralapati S. Determination of nicotine in tobacco, tobacco processing environments and tobacco products. In: Gorrod JW, editor. Analytical determination of nicotine and related compounds and their metabolites. Amsterdam: Elsevier; 1999. p. 285–391.
- Norman A, Jones EG. The history of cigarette design. Recent advances in tobacco science—responding to changes in our industry, vol 24. Atlanta, GA: Tobacco Science Research Conference; 1998. pp. 13–6.
- Stevenson T, Robert NP. The SECRET and SOUL of Marlboro: Phillip Morris and the origins, spread, and denial of nicotine freebasing. *Am J Public Health*. 2008;98:1184–94.
- Camino G, Costa L. Intumescent fire-retardant systems. *Polym Degrad Stab*. 1989;23:359–76.
- Tzamtzis A, Pappa A, Mourikis A. The effect of  $(\text{NH}_4)_2\text{HPO}_4$  and  $(\text{NH}_4)_2\text{SO}_4$  on the composition of the volatile organic pyrolysis products of *Pinus halepensis* pine-needles. *Polym Degrad Stab*. 1999;66:55–63.
- Suardana NPG, Ku MS, Lim JK. Effects of diammonium phosphate on the flammability and mechanical properties of bio-composites. *Mater Des*. 2011;32:1990–9.
- Nama S, Condon BD, Parikha DV, Zhao Q, Cintróna MS, Madison C. Effect of urea additive on the thermal decomposition of greige cotton nonwoven fabric treated with diammonium phosphate. *Polym Degrad Stab*. 2011;96:2010–8.
- Levchik SV, Balabanovich AI, Levchik GF, Costa L. Effect of melamine and its salts on combustion and thermal decomposition of polyamide 6. *Fire Mater*. 1997;21:75–83.
- Zhou S, Wang ZZ, Gui Z, Hu Y. Flame retardation and thermal degradation of flame-retarded polypropylene composites containing melamine phosphate and pentaerythritol phosphate. *Fire Mater*. 2008;32:307–19.
- Chen WY, Wang YZ, Chang FC. Thermal and flame retardation properties of melamine phosphate-modified epoxy resins. *J Polym Res*. 2004;11:109–17.
- Zhou S, Xu Y, Wang CH, Tian ZF. Pyrolysis behavior of pectin under the conditions that simulate cigarette smoking. *J Anal Appl Pyrolysis*. 2011;91:232–40.
- Buryan P, Staff M. Pyrolysis of the waste biomass. *J Therm Anal Calorim*. 2008;93:637–40.
- Gani A, Naruse I. Effect of cellulose and lignin content on pyrolysis and combustion characteristics for several types of biomass. *Renew Energy*. 2007;32:649–61.
- Shen DK, Gu S, Luo KH, Wang SR, Fang MX. The pyrolytic degradation of wood-derived lignin from pulping process. *Bioresour Technol*. 2010;101:6136–46.
- Hajaligol MR, Waymack B, Kellogg D. Formation of aromatic hydrocarbons from pyrolysis of carbohydrates. *Prepr Pap Am Chem Soc Div Fuel Chem*. 1999;44:251–5.
- Zhijia L, Benhua F, Zehui J, Zhiyong C, Yan Y, Xing L. A comparative study of thermal properties of sinocalamus affinis and moso bamboo. *J Therm Anal Calorim*. 2012. doi:10.1007/s10973-012-2266-x.
- Teixeira KC, Moreira GF, Quirino WG, Legnani C, Silva RA, Cremona M, Brito HF, Achete CA. TG–FTIR thermal stability investigation of tetrakis beta-diketonates complexes. *J Therm Anal Calorim*. 2011;106:587–93.
- Li J, Wang Z, Yang X, Hu L, Liu Y, Wang C. Evaluate the pyrolysis pathway of glycine and glycyglycine by TG-FTIR. *J Anal Appl Pyrolysis*. 2007;80:247–53.
- Shuang H, Yuan H, Lei S, Hongdian L. Effect of modified organic–inorganic hybrid materials on thermal properties of cotton fabrics. *J Therm Anal Calorim*. 2011;103:423–7.
- Amen-Chen C, Pakdel H, Roy C. Production of monomeric phenols by thermochemical conversion of biomass: a review. *Bioresour Technol*. 2001;79:277–99.
- Shen DK, Gu S. The mechanism for thermal decomposition of cellulose and its main products. *Bioresour Technol*. 2009;100:6496–504.
- Johnson WR, Rale RW, Clough SC, Chen PH. Chemistry of the conversion of nitrate nitrogen to smoke products. *Nature*. 1973;243:223–5.
- Wang ZZ, Lv P, Hu Y, Hu K. Thermal degradation study of intumescent flame retardants by TG and FTIR: melamine phosphate and its mixture with pentaerythritol. *J Anal Appl Pyrolysis*. 2009;86:207–14.
- Richard EL, Richard NW. Pyrolysis combustion flow calorimetry. *J Anal Appl Pyrolysis*. 2004;71:27–46.
- Schartel B, Bartholmai M, Knoll U. Some comments on the use of cone calorimeter data. *Polym Degrad Stab*. 2005;88:540–7.